IMAGING OF NON-RESOLVED OBJECTS USING THE FINE SCALE OPTICAL RANGE

Thomas C. Pollock, Peter M. Grubb
Space Engineering Research Center, Texas A&M University
MS 3118 College Station, TX 77843-3118

ABSTRACT

The Fine Scale Optical Range (FiScOR) has been designed and assembled at the Space Engineering Research Center(SERC) at Texas A&M University to study the efficacy of on-orbit debris characterization using small space-based cameras. Physically, this facility permits imaging of small, one to two centimeter models of simple or complex shapes from a distance sufficiently great to produce image sizes of about one pixel. The objects are designed in 3D CAD and produced in plastic by 3D printing. They are then surfaced with real materials such as multi-layer insulation (MLI) and silicon solar cell fragments. Details, such as slight faceting in solar cell arrays, are achieved to dimensions as fine as 200 micrometers. Mechanisms are provided to rotate and translate the object. Illumination sources approximating the solar spectrum are used. Light curves are recorded using CCD or CMOS cameras which may be cooled or operated at ambient temperature. This research supports a more extensive body of work for the Air Force Research Lab and others examining image processing with noise terms for cameras imaging in visible and near-visible light, and assessing operational effects using synthetic space images created in the lab.

1. INTRODUCTION

High fidelity computer generated simulated digital images are useful tools in the camera design process, because they allow the designer to see the effects of design changes on image quality. In addition to the usual camera size parameters, four models are essential to the simulation: detector noise, lens point spread function (PSF), background, and the object of interest. Here, one system for modeling certain objects of interest is presented.

Several requirements are recognized. First, it is essential that the system be able to support camera-in-the-loop experiments. This requires that the system feature either physical 3D models or computer-generated shapes that can be displayed on a flat panel monitor placed in the field of view of the camera. Second, because the primary interest is simulation of small spaced-based cameras tasked with detecting resident space objects (RSOs), the scale of interest corresponds to a distant point source. Third, modeling the interaction of light with the object surfaces must be as near to perfect as possible, including color. Fourth, the system must support translation and rotation of the model. An extensive trade study of both kinds of models concluded that the use of small scale 3D physical models is a viable approach, so long as the distance from the camera to the model, L, is sufficiently great that the model appears as a point on the image plane. In practical terms, this means that for a given L, the model size, h_0, must be chosen to obtain an image size that is less than the radius of the Airy disk, h_1. Combining the well known Airy disk and thin lens equations provides a scaling law relating model size to object distance, d_0, focal length, f, and aperture diameter, ϕ:

$$h_0 = \frac{1.22 \cdot \lambda \cdot (d_0 - f)}{\phi} \tag{1}$$

As is seen in Eq. 1, smaller aperture permits larger models. Choosing $d_0 = 50$m and $f = 100$mm gives a model size of about 1 cm, with the lens stopped to $\phi = 3$mm . Admittedly, the small aperture is not representative of flight hardware, but it must be remembered that this experiment is designed to obtain light curves of rotating, translating RSO models and that the scale must be convenient to the available laboratory space. This work is directed specifically toward the use of small cameras—star tracker size, perhaps—to search for RSOs. [1]

Accordingly, a series of experiments have been completed based on a working distance of 50m and a model scale of approximately 1 cm. Reported herein are results obtained using one camera and four models. The models are cubes,

each of which have all six surfaces finished identically. We regard these experiments as representing proof of the concept introduced above.

We regard this work to be proof of concept and, as such, is not an exhaustive survey of surface material, rotation axis, source phase or camera position.

2. METHOD

The experiment was assembled in a confined space using a number of fold mirrors. The layout is shown in Fig.1. The arrangement is not ideal, but it is adequate for present work. The mirrors are small: most are 35 x 25mm in size. All are first surface 1/4 λ PV with antireflective coatings. Because the edges of the mirrors appear within the FOV of most of our cameras, all are apodized.

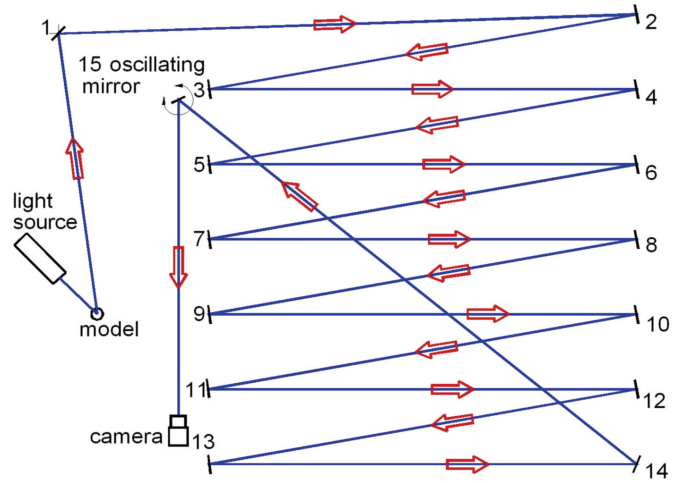

Fig. 1: The optical path is folded into a 4 x 5m footprint.

Mirror 15 is fixed to a zero backlash oscillating base which produces the translation. The model is mounted on a rotating base. Both motions are variable speed, controlled by computer using National Instruments LabVIEW ® software.

The light source is a quartz halogen lamp with fiber optic output, a collimating lens and a baffle designed to approximate the angular size of the Sun. It is adequate for current purposes, but its spectrum differs significantly from the Sun, as seen in Fig. 2.

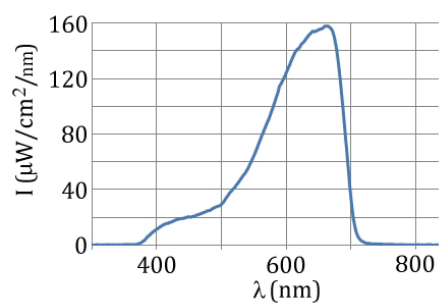

Fig. 2: Light source spectrum, including NIR cut filter.

The camera used in this study is a COTS CMOS Silicone Imaging® SI640-HFRGB mated to a Canon 85mm f/1.2 lens. This combination is chosen for its high frame rate (200 fps) color (Bayer mask), high data rate Camera Link interface and fast optics. An EPIX PIXCI® EB1 interface card and EPIX XCAP® software is used for frame grabbing. The imaging rate is approximately 400 frames per revolution of the model. Integration time is 15ms.

Four ABS polymer cube models were produced using a combination of 3D printing [2,3] and CNC operations. Each was fitted with a metal stalk which passed through the model along paths as drawn in Fig. 3. They were initially painted white using a TiO_2–rich acrylic lacquer.

After imaging each model, three of the four cubes were resurfaced in other materials. Two of them were surfaced with solar cells. Each face of Cube 2 was covered with a single piece of solar cell material. An effort was made to minimize fracturing of these pieces, but some fine fracture lines were observed after the adhesive was fully cured. The adhesive, a rigid epoxy, held the fractured surfaces in very nearly coplanar positions. Cube 3 was also surfaced with solar cell material. To model real solar arrays more precisely, the material was intentionally fractured to produce a distribution of attitudes. An elastomeric adhesive was used to mount unfractured pieces. When partially cured, the adhesive permitted fracturing into small fragments roughly 1mm in size. No attempt was made to ground solar cell electrodes. Cell edges were painted black to eliminate spurious glints. Cube 4 was resurfaced in aluminum foil. Again, an elastomeric adhesive was used, resulting in a wrinkled appearance. After resurfacing, the imaging sequence was repeated.

For comparison with the white cubes, Phong [4] models were generated using DesignCAD® 3D solid modeling software. Note that the Phong algorithm is not physics-based. Separate sources, specular, diffuse and ambient, are

defined. Only the specular source can produce a specular reflection; diffuse produces diffuse and ambient produces ambient. So to simulate reality, one must have prior knowledge of the intensities of the three sources.

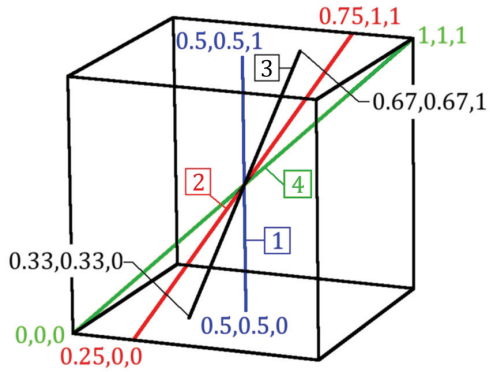

Fig. 3: Rotation axes of the four cubes.

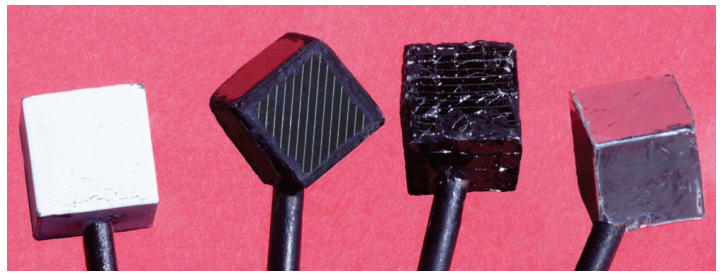

Fig. 4: The four cubes as surfaced/resurfaced. From left, (1) remains white, (2) is solar cell, (3) is fractured solar cell and (4) is wrinkled aluminum.

Camera position and attitude remained constant throughout, with the lens paraxial ray (the line from the model to Mirror 1) aligned in the working plane (the plane formed by the locations of the centers of all mirrors) as shown in Fig.1. The light source is located below the working plane and is angled upward toward the model at an elevation angle of 16.5°. Light source azimuth angle is measured counterclockwise from the paraxial direction; angles chosen are 10°, 45°, 90° and 135°.

3. RESULTS AND DISCUSSION

Nearly 14,000 images form the raw data. Thanks to in-camera windowing, nearly all of the images are just 32 x 32 pixels in size. Brightness resolution is 8-bits per color. Image processing is simple. There are 7 objects and four lighting angles, resulting in 28 image sets. Each image is reduced to three numbers: the sums of the ADU of R, G and B. No noise reduction is performed. These numbers are plotted in sequence to produce a light curve. For brevity, only a representative selection of the curves are presented here. Curves are grouped in a fashion which supports the discussion to follow.

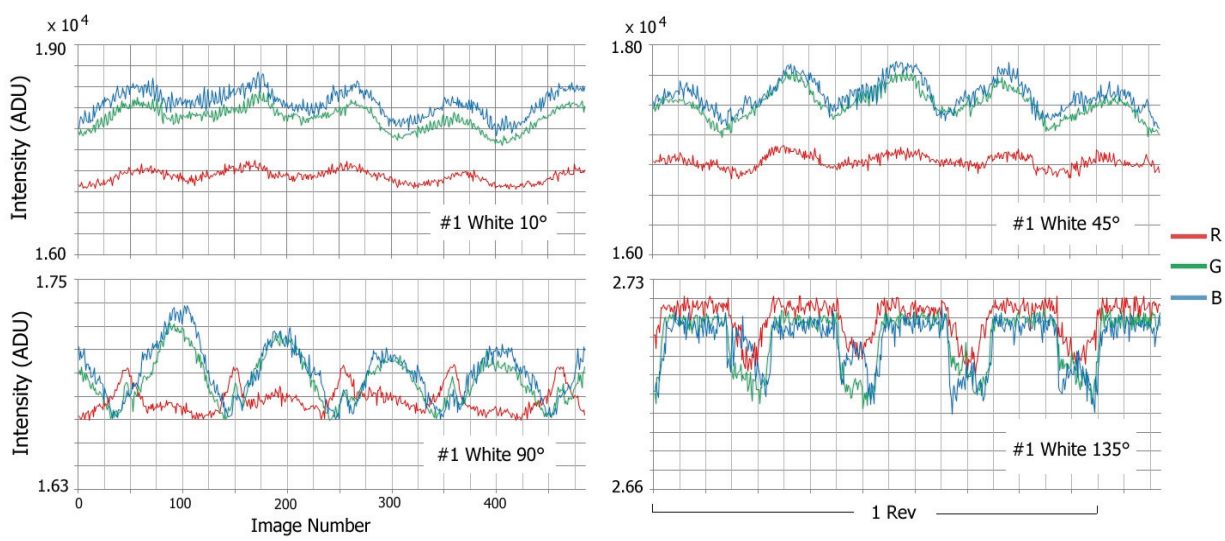

Fig. 5: Cube 1, white, four lighting angles.

Fig. 5 presents all of the data obtained from Cube 1, the geometry of which, combined with the light source elevation angle of 16.5° prevents specular rays from being recorded regardless of the azimuth angle. Several features are worthy of note, Most obvious is that R has lower reflectivity and sensitivity than G and B. From Fig. 2 we know that the source is strongest in R. The 90° azimuth shows a curious reversal in intensity in R only. At 135°, all three colors are much brighter than in the other three curves, which is expected from the glancing angle and the smooth lacquer surface.

Figs. 6 - 13 form a comparison between two different surfaces applied to the same cube. The geometry of this cube should produce a strong specular reflection near 90° azimuth. Indeed, the solar cell material (Fig. 11) is strongly specular under this lighting condition, and the white painted surface (Fig. 10) also shows increased intensity. The white cube again shows lower reflected intensity and sensitivity in R while the solar cell finish does not, but the noise floor is about 1.35 x 10^4 ADU so one cannot deduce whether there is a similar phenomenon occurring in the solar cell covered model.

Fig. 12 shows the same overall increase in intensity as seen in Fig. 5 at 135°, but Fig. 13 does not. Apparently, the reflected energy is nearly all specular in the latter case. The solar cells have an SiO antireflective coating, but this is not effective at glancing angles. Evidence of specular reflections from the white paint surface is also seen in Fig. 12.

Figs. 14 and 15, Cube 3 with fractured solar cells, should be somewhat noisier than Cube 2, unfractured cells. Visually, this appears to be the case, but a complete bidirectional reflectance distribution function (BRDF) [5] survey is required before a meaningful statistical result can be obtained.

Figs. 16 -19 present data from Cube 4, aluminum surface. Note that the R intensity is lower than G and B. Recall that this was also observed in the white models. The shiny surfaces of this cube should reflect all colors equally, so the data suggest that the camera's color balance is biased toward the blue end of the spectrum. Cube 4, white, is compared to a Phong model in Fig.20. We chose the 90° azimuth to illustrate the difference between white and aluminum (Fig. 18). Three-fold symmetry is seen in both materials, but diffuse broadening is obvious in the white model and absent in the aluminum as expected.

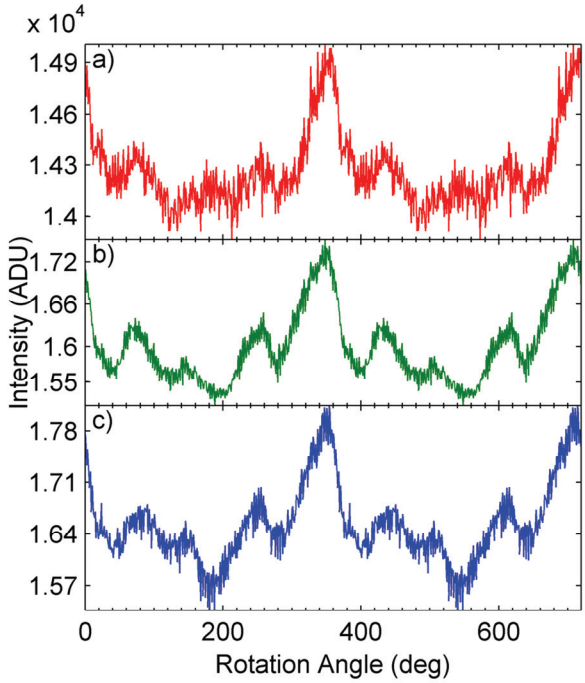

Fig.6: Cube 2, white finish, 10° lighting.

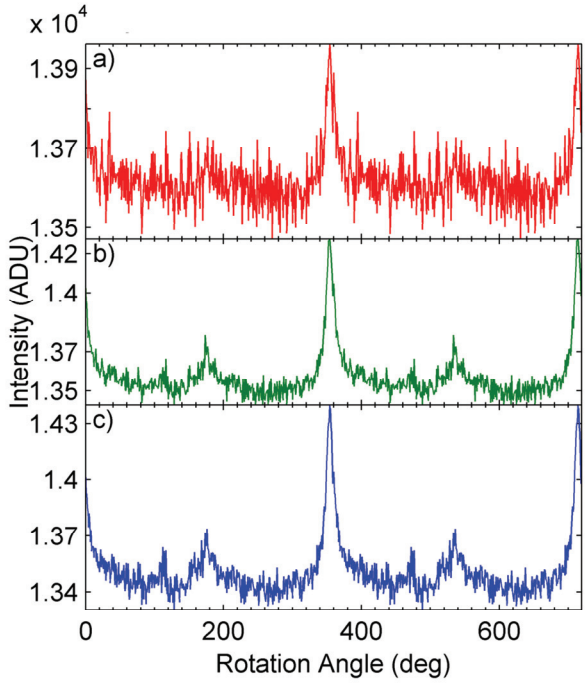

Fig. 7: Cube 2, solar cell finish, 10° lighting.

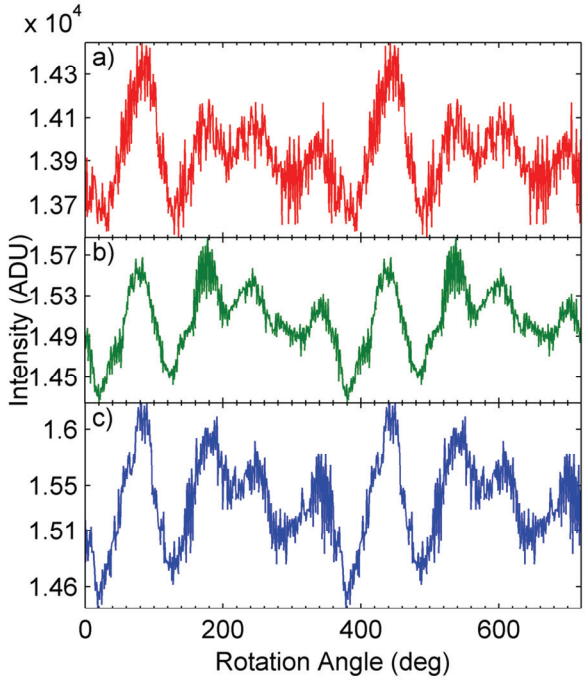

Fig. 8: Cube 2, white finish, 45° lighting.

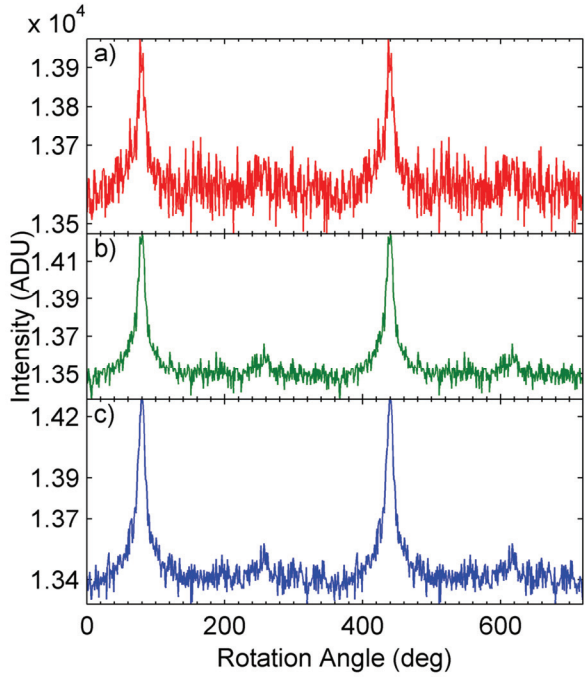

Fig. 9: Cube 2, solar cell finish, 45° lighting.

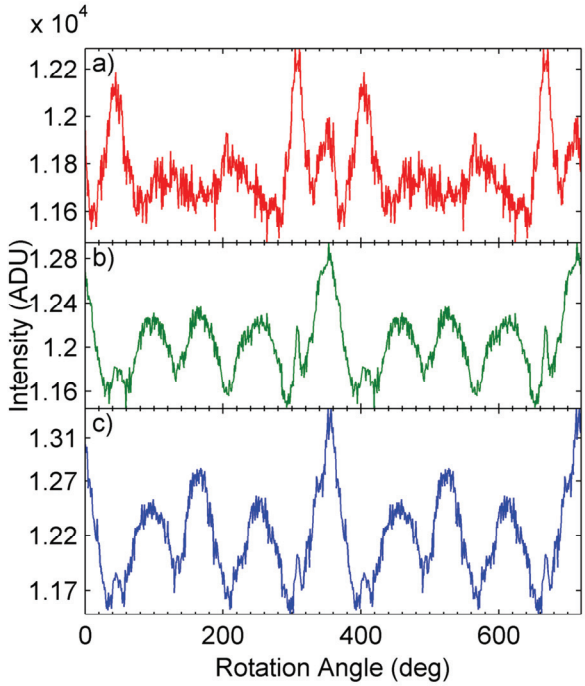

Fig. 10: Cube 2, white finish, 90° lighting.

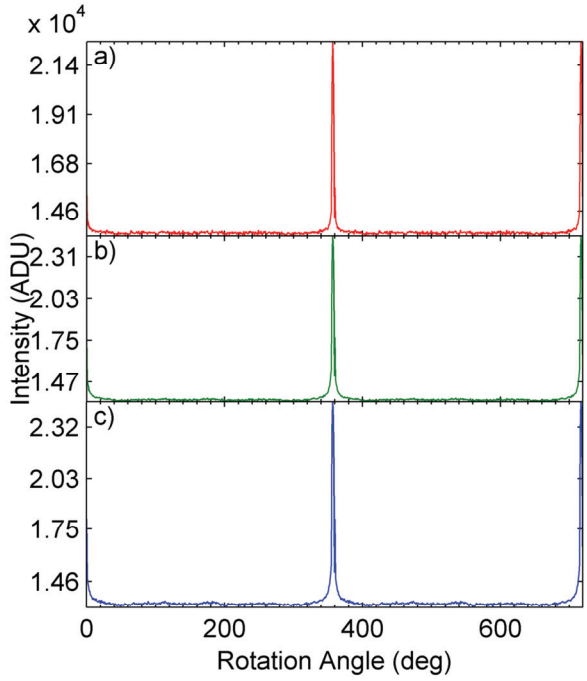

Fig. 11: Cube 2, solar cell finish, 90° lighting.

Phong models were generated for all of the white cubes. For brevity, we present only one result, Fig. 20. This result has a slightly higher correlation between Phong and physical surface than is typical but in general, all of the

correlations were good. Note that there is a marked disagreement between the smaller measured maxima and the corresponding features in the Phong model, which are minima. Earlier we referred to a curious feature in Fig. 5: a maximum in R where a minimum is expected. Phong also predicts a minimum at this location, which we offer as justification of our method.

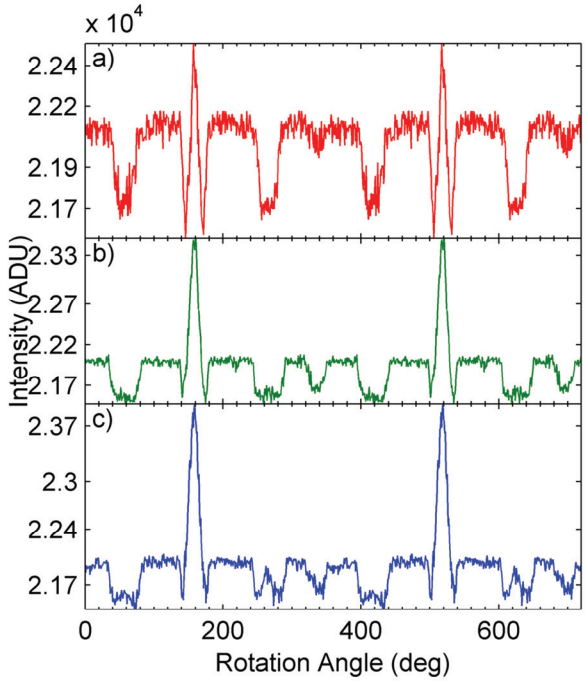

Fig. 12: Cube 2, white finish, 135° lighting.

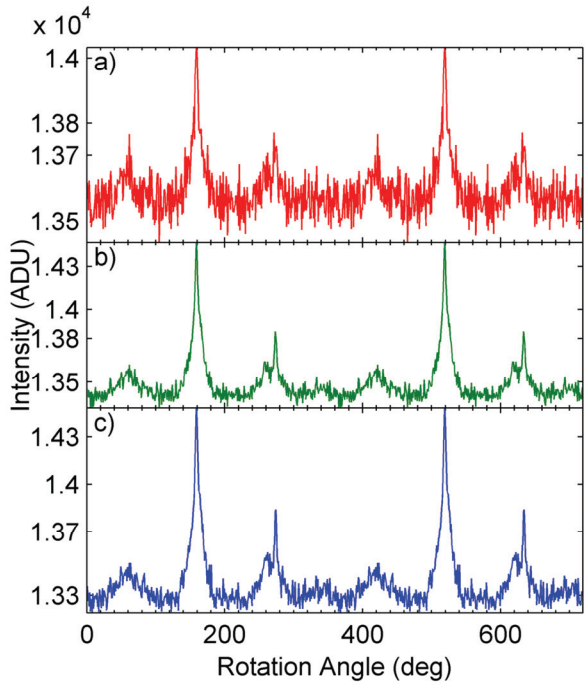

Fig. 13: Cube 2, solar cell finish, 135° lighting.

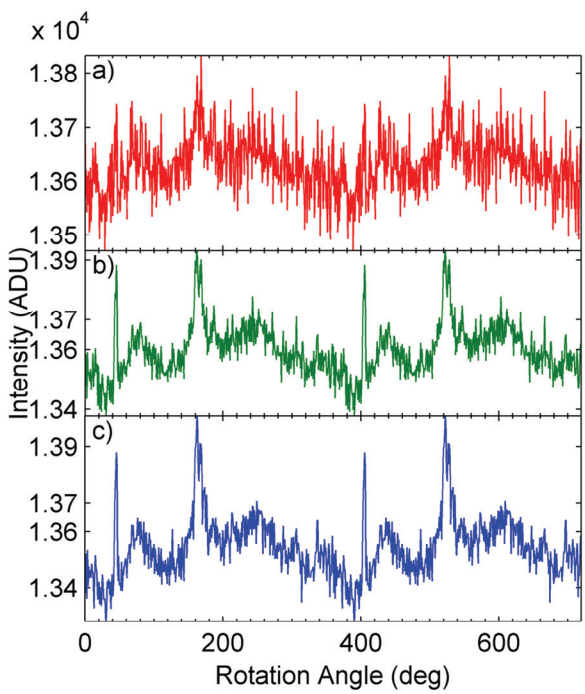

Figure 14: Cube 3, fractured solar cell, 10° lighting.

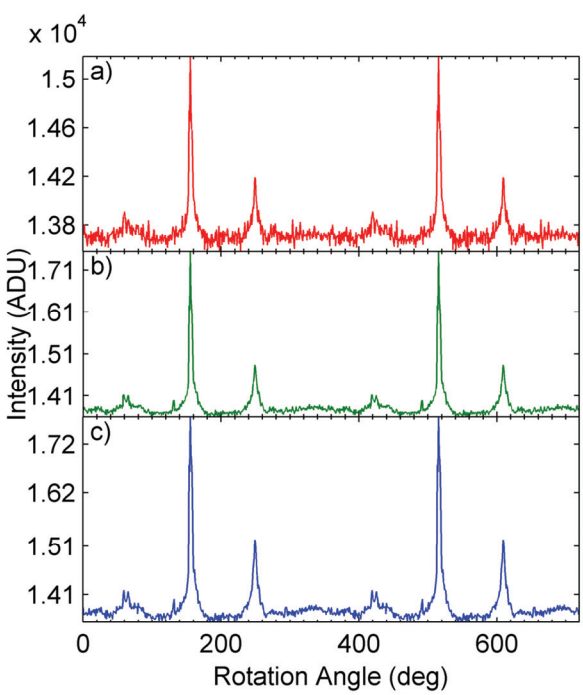

Figure 15: Cube 3, fractured solar cell, 45° lighting.

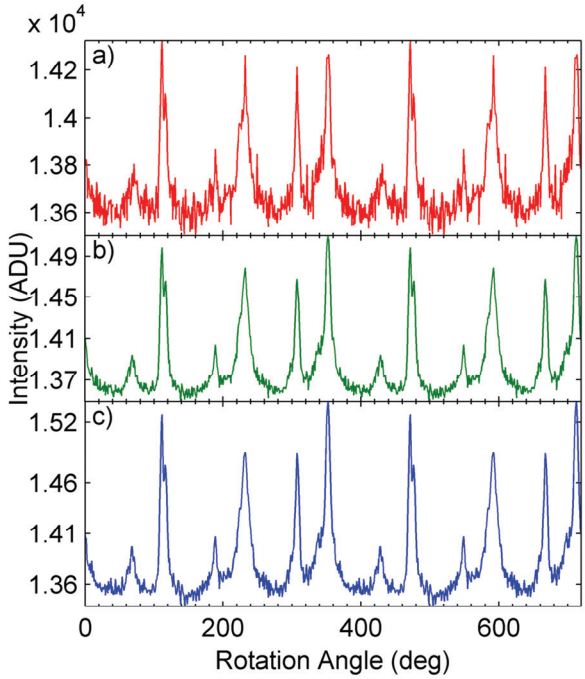

Figure 16: Cube 4, aluminum surface, 10° lighting.

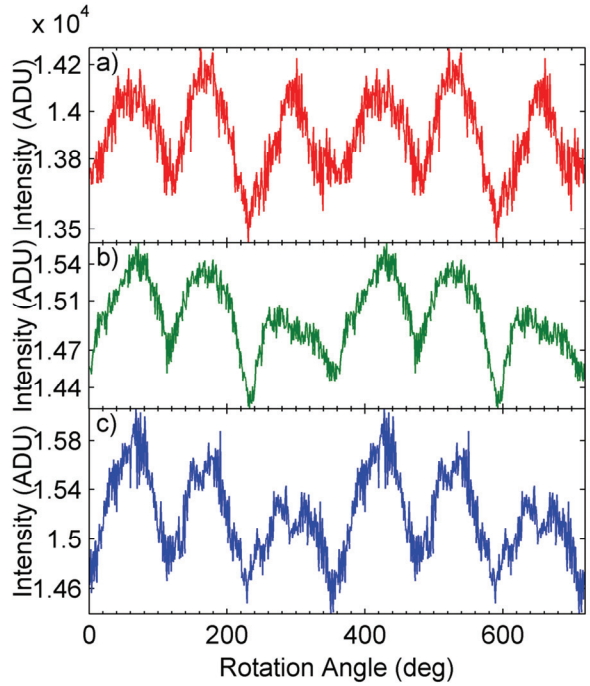

Figure 17: Cube 4, aluminum surface, 45° lighting.

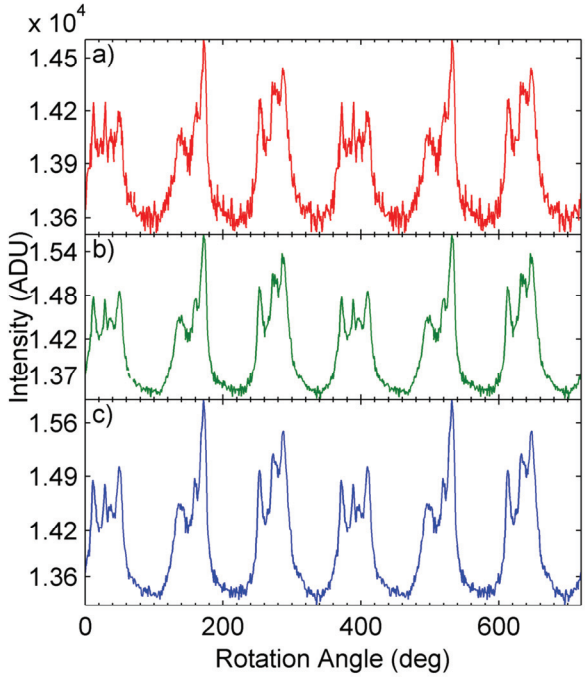

Figure 18: Cube 4, aluminum surface, 90° lighting.

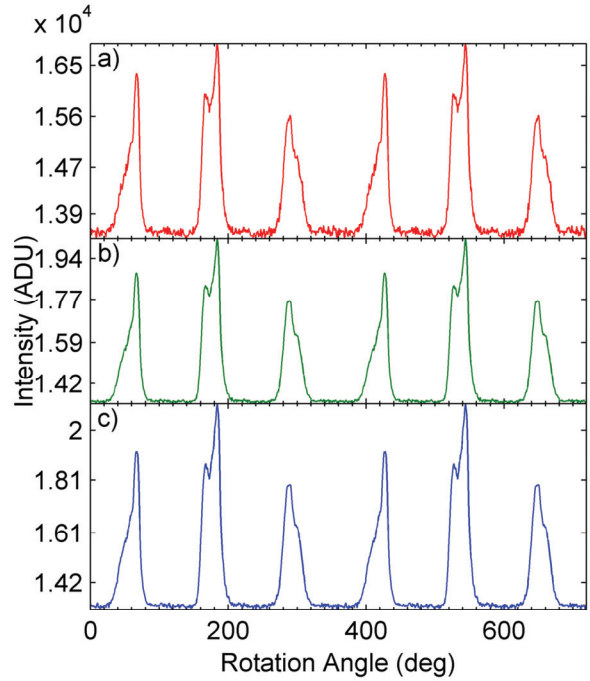

Figure 19: Cube 4, aluminum surface, 135° lighting.

Some general comments are in order. Throughout these experiments, source intensity is low enough that no pixels were saturated in any image, but high enough to prevent noise from dominating the data. Noise levels are somewhat higher in R than in G orB, which are comparable.

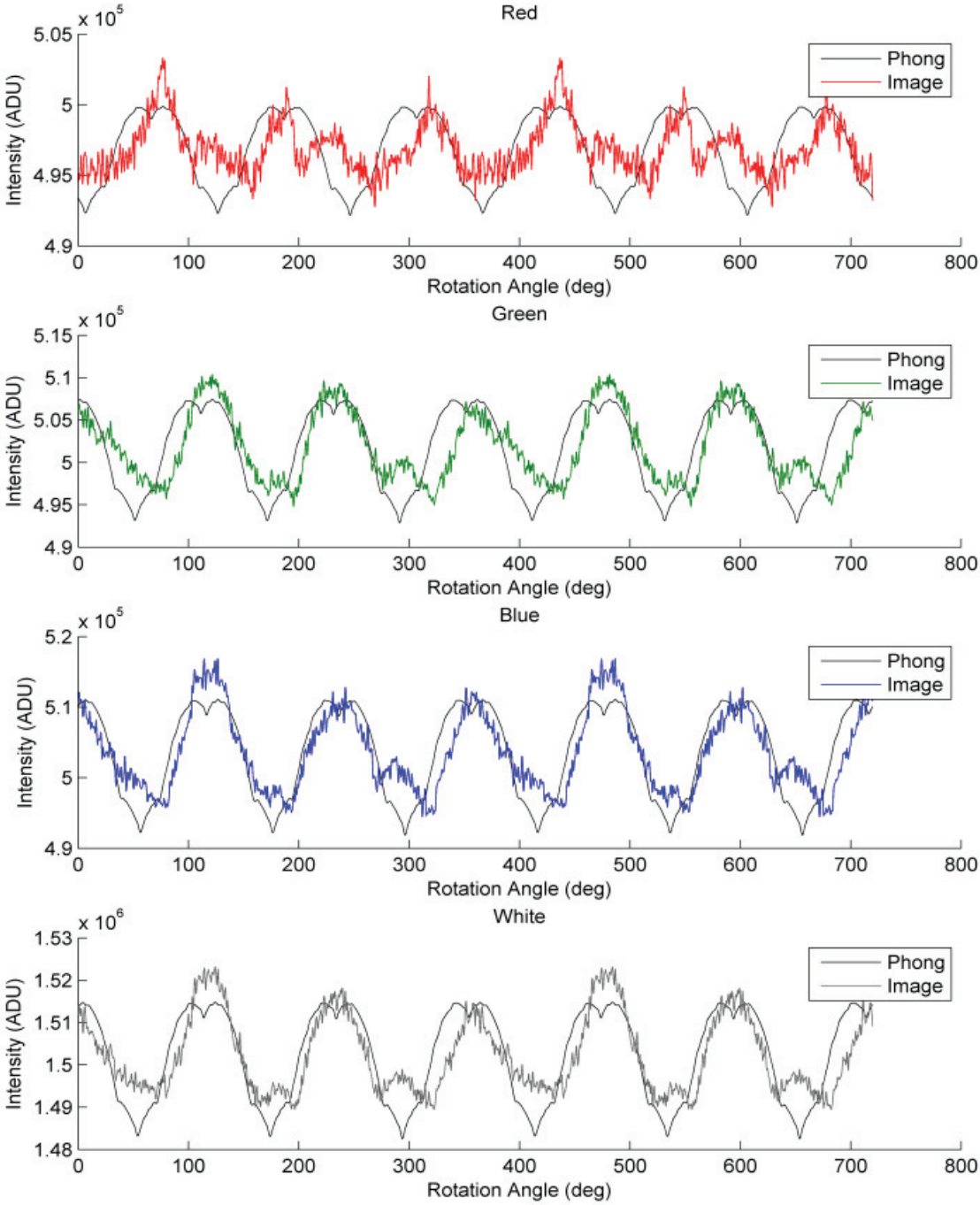

Fig. 20: Cube 4, white. LRGB and Phong model, 90° lighting. The intensity values on these curves are a factor of 32 higher than the previous figures. This is a feature of the Phong modeling code. The images are not brighter than the previous.

In nearly every model, there are noticeable differences among the R, G and B curves, suggesting that there is merit to imaging in color. Sometimes, as seen in Fig. 10, the difference is quite pronounced.

The many small mirrors are, in most respects, a disadvantage. They broaden and alter the shape of the PSF somewhat, and are too small to support any work with extended objects. An advantage of the compact layout is thermal uniformity, which requires attention in the design of long tunnels.

Preparation of small models is tedious artwork requiring extensive knowledge of art materials and practices, as well as fine motor skills. Scaling on the order of 4cm, as opposed to 1cm, would be preferred, but per Eq. 1, the range length increases to 200m.

4. CONCLUSIONS

1. The concept of generating realistic light curves from images of small physical models is proven. The four materials/shapes gave recognizably different curves. This was the expected outcome. A refrigerator is larger than a sugar cube but both are much larger than the wavelength of light. Compact images of the two should be equivalent, and videos of their rotations should reveal information about their geometry and materials. One caveat: we chose the scale to ensure "point" images and Fraunhofer diffraction conditions. The method reported here should be assumed to apply to extended objects.
2. Information in R, G and B channels differ significantly, indicating that imaging in color may be beneficial in material identification. A more Sun-like light source and a color-calibrated camera are required for quantitative analysis.

5. ACKNOWLEDGEMENTS

The authors would like to thank Charles Hill, Director, Space Engineering Research Center (SERC), Texas A&M University, for providing laboratory space and some of the equipment for this work. We greatly appreciate the encouragement of Drs. Moriba Jah and Brien Flewelling of AFRL. In addition, we thank Texas A&M University's Research Opportunities for Engineers Scholarship program for funding one of us (PMG). Finally, special thanks are due to Dr. Christian Bruccoleri , Assistant Director of SERC, for Matlab coding help and generous assistance throughout the project.

6. REFERENCES

1. Ettouati, I., Mortari, D., and Pollock, T.C. "Space Surveillance Using Star Trackers: Simulations," Paper AAS 06-231 of the 2006 AAS Space Flight Mechanics Meeting Conference, Tampa, FL, January 22-26, 2006.
2. Chee Kai Chua; Kah Fai Leong, Chu Sing Lim (2003). Rapid Prototyping. World Scientific. p. 124. ISBN 978-981-238-117-0.
3. ASTM F2792-10 Standard Terminology for Additive Manufacturing Technologies, copyright ASTM International, 100 Barr Harbor Drive, West Conshohocken, PA 19428.
4. Phong, B. T., Illumination for computer generated pictures, Communications of ACM 18 (1975), no. 6, 311–317.
5. Bowers, D.L. et al, Broadband Spectral-Polarimetric BRDF Scan System and Data for Spacecraft Materials, AMOS, 2011.